

# Multiobjective Optimization of Steam Reformer Performance Using Genetic Algorithm

J. K. Rajesh, Santosh K. Gupta,<sup>†</sup> G. P. Rangaiah, and Ajay K. Ray\*

Department of Chemical and Environmental Engineering, National University of Singapore, 10 Kent Ridge Crescent, Singapore 119260, Singapore

An existing side-fired steam reformer is simulated using a rigorous model with proven reaction kinetics, incorporating aspects of heat transfer in the furnace and diffusion in the catalyst pellet. Thereafter, “optimal” conditions, which could lead to an improvement in its performance, are obtained. An adaptation of the nondominated sorting genetic algorithm is employed to perform a multiobjective optimization. For a fixed production rate of hydrogen from the unit, the simultaneous minimization of the methane feed rate and the maximization of the flow rate of carbon monoxide in the syngas are chosen as the two objective functions, keeping in mind the processing requirements, heat integration, and economics. For the design configuration considered in this study, sets of Pareto-optimal operating conditions are obtained. The results are expected to enable the engineer to gain useful insights into the process and guide him/her in operating the reformer to minimize processing costs and to maximize profits.

## Introduction

Steam reforming of hydrocarbons has been in use for several years as the principal process for the generation of hydrogen and synthesis gas needed in the chemical industry. The popularity of this process can be attributed to its higher processing efficiency and cost-effectiveness in comparison to competing processes. Today, natural gas is the most common feedstock for steam reforming, being used in more than 75% of the operating units.<sup>1</sup> In the future, deteriorating quality of crude oils, stringent petroleum product specifications, and environmental regulations will lead to increased demands for hydrogen (for hydroprocessing in petroleum refineries), and increasing competition will require more efficient design and operation of steam reformers. Optimal operation of existing steam reformers is crucial in view of the high energy consumption and large value addition involved in the process. Often, several objectives and constraints are involved in any real-life unit, and optimization studies incorporating these conflicting requirements would be invaluable to the process engineer. In this work, we obtain optimal operating conditions for an industrial reformer with two objective functions and an end-point constraint, using genetic algorithm (GA).

The theoretical and practical aspects of steam reforming have been dealt with comprehensively by Rostrup-Nielsen<sup>2</sup> and Ridler and Twigg.<sup>3</sup> Extensive studies on the kinetics and reaction mechanism of steam reforming have been reported in the open literature. Elnashaie and co-workers<sup>4,5</sup> have presented excellent reviews of past works in this area. Xu and Froment<sup>6</sup> obtained a generalized Langmuir–Hinshelwood type kinetic model considering the water–gas shift reaction to occur in parallel with the steam reforming reactions. They<sup>7</sup>

validated their kinetics by successfully using it to simulate an industrial reformer. Their kinetic model has since gained wide acceptance<sup>5</sup> and is considered adequate to model industrial steam reformers. Early efforts<sup>8</sup> underlined the significance of mass-transfer resistances to reaction within the catalyst pellet. These studies indicated very low effectiveness factors, implying that only a thin layer of catalyst close to the surface contributed to the reaction. This prompted later workers<sup>7,9</sup> to shift from pseudo-homogeneous reactor models to heterogeneous models, in which they showed that effectiveness factors for some of the reactions were negative. Soliman et al.<sup>10</sup> studied the effect of important operating and design variables on the performance of a reformer. In the past, Hyman<sup>11</sup> modeled an industrial reformer considering reforming and shift conversion as elementary reactions. In this model, he assumed a tube wall temperature profile and then solved the mass and energy balances inside the tube. Singh and Saraf<sup>12</sup> presented a detailed model of a side-fired reformer with an empirical kinetic model, including the radiative transfer of heat to the tubes in the energy balance calculations. Plehiers and Froment<sup>13</sup> developed a reformer simulation program which used the zone method and Monte Carlo simulation techniques to compute the radiative flux in the furnace. Trimm<sup>14</sup> analyzed the mechanism of coke formation during steam reforming and suggested operational strategies to minimize coking.

In contrast to the extensive work reported in the open literature on the modeling and simulation of steam reformers, work on their optimization is limited. Hosain<sup>15</sup> identified optimal operating conditions for the reformer, which maximized the conversion of methane. He used thermodynamic equilibrium considerations in his work because most reformers give near-equilibrium products. Elnashaie et al.<sup>16</sup> analyzed the nonmonotonic kinetics of steam reforming and predicted the existence of an optimum partial pressure of steam in the feed for maximizing the conversion of methane. Wagner and Froment<sup>17</sup> addressed the need to select the steam-to-carbon ratio,  $(S/C)_{in}$ , in the feed to minimize the

\* Corresponding author. Tel: (65) 874 8049. E-mail: cheakr@nus.edu.sg. Fax: (65) 779 1936.

<sup>†</sup> On leave from Indian Institute of Technology, Kanpur 208016, India. Present address: Department of Chemical Engineering, University of Wisconsin, Madison, WI 53706.

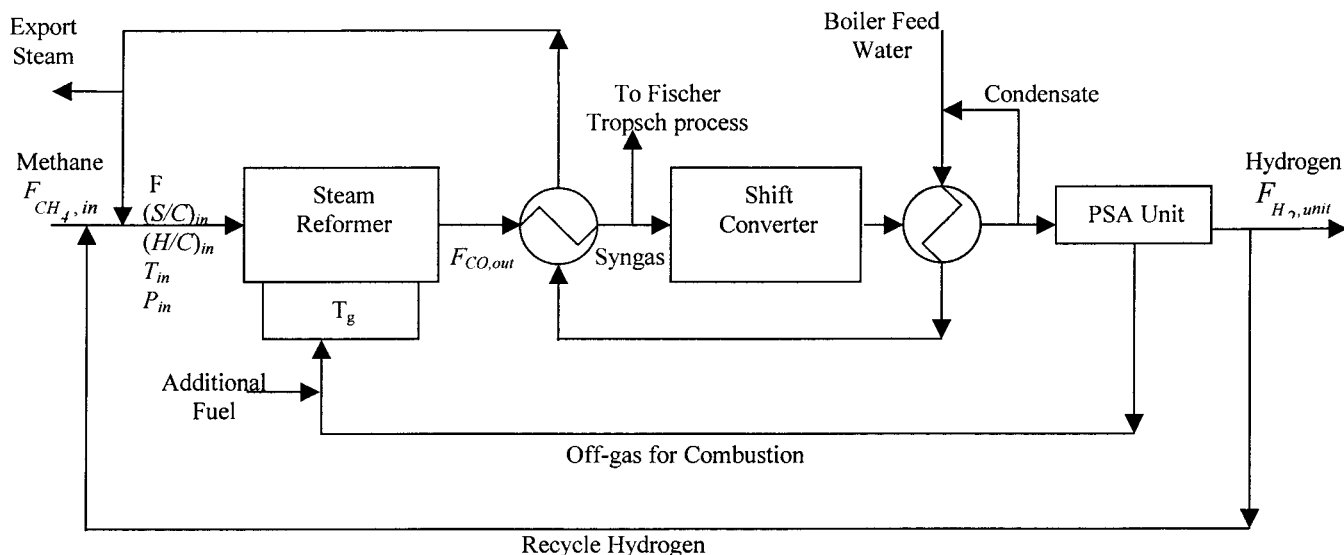
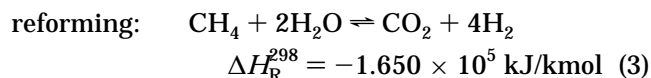
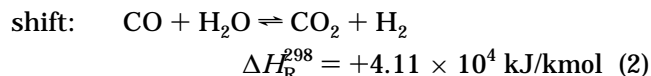
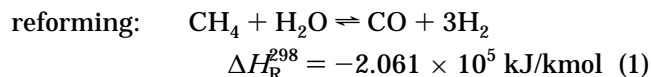


**Figure 1.** Process flow diagram for the steam reforming of methane.

reformer dimensions, while simultaneously eliminating coke formation. They obtained the lowest possible value of  $(S/C)_{in}$  for safe, coke-free operation. Zhang and Yu<sup>18</sup> used the kinetic model of Hyman<sup>11</sup> with a detailed heat-transfer model for a top-fired reformer. They optimized the energy consumed in the reformer furnace using this model. Hohmann<sup>19</sup> indicated the reactor conditions which favor coking reactions and those wherein the reverse reaction "gasification" is favored. Farnell<sup>20</sup> presented case studies to show how simulation packages could be used to reconcile plant data and assess the scope for improvement in reformer operation. All of the optimization studies reported up to now involved a single objective function only. To the best of our knowledge, the present work is the first attempt to study optimization of steam reformers using multiple-objective functions and constraints.

### Problem Formulation

**Process Description.** Figure 1 shows a typical flowsheet of the steam reforming process. Natural gas (assumed to be pure methane in this study) is mixed with appropriate quantities of steam and recycle hydrogen before entering the reformer furnace. The recycle of some of the  $H_2$  produced to the feed is necessary because  $H_2$  is essential to keep the catalyst in the early part of the reformer tubes in the reduced (active) state. The following are the important reactions taking place:



Of these, the two reforming reactions occur (in parallel) primarily in the steam reformer (first reactor) while thermodynamics favor the shift reaction in the near-adiabatic shift converter (second reactor). The hot syngas produced in the reformer is used to generate very high pressure (VHP) steam used for mixing with the

feed (internal use) as well as for "export" outside the unit. In the design and operation of reformers, generation of VHP steam for export is given almost the same importance in industry as the production of  $H_2$ . The cooled syngas goes to the shift converter, operating at lower temperatures, where additional  $H_2$  is produced. The  $H_2$ -rich exit stream from the shift converter is cooled, and then  $H_2$  is separated from the off-gases in a pressure-swing adsorption (PSA) unit. The off-gas, with additional fuel, is used for combustion in the reformer furnace.

The extent of the two endothermic reforming reactions is controlled largely by the rate of heat transfer from the furnace to the catalyst pellets and reacting gases inside the reformer tubes and also by the severe diffusional resistances which are present inside the porous catalyst pellets. Both of these important aspects must be incorporated in any model of the reformer.

**Reformer Model.** In the present study, the reaction model of Xu and Froment<sup>6</sup> is used without any modifications (to the kinetic scheme and rate constants) because this model has been very successful in simulating industrial reactors.<sup>5</sup> The model of Singh and Saraf<sup>12</sup> for heat transfer from the furnace to the tubes is adapted slightly to make the computation of the tube wall temperature profile noniterative. The catalyst pellet is assumed to be isothermal, with its temperature being the same as the gas temperature at that axial location.<sup>5</sup> The method of orthogonal collocation (OC) on finite elements<sup>21,22</sup> is used to obtain the intrapellet concentration profiles and the effectiveness factors at any axial location in the reactor. Two finite elements extending over  $0 \leq v \leq 0.2$  (outer region) and  $0.2 \leq v \leq 1.0$  (inner region) are used in the catalyst pellet (modeled as a slab<sup>5</sup>). Eighteen OC points are assumed in the first finite element. The flux at  $v = 0.2$  is assumed to be zero for all of the components. This implies that equilibrium exists in 80% (the inner region) of the catalyst slab, taken as the second finite element. The computed results were found to be consistent with the net reaction rates being zero for  $v \geq 0.2$ . This technique is a simplification of that used by Xu and Froment,<sup>6</sup> who used three finite elements and a total of 22 OC points. The simplified model II of Elnashaie et al.<sup>5</sup> is used for the computation of the effective diffusivities and sim-

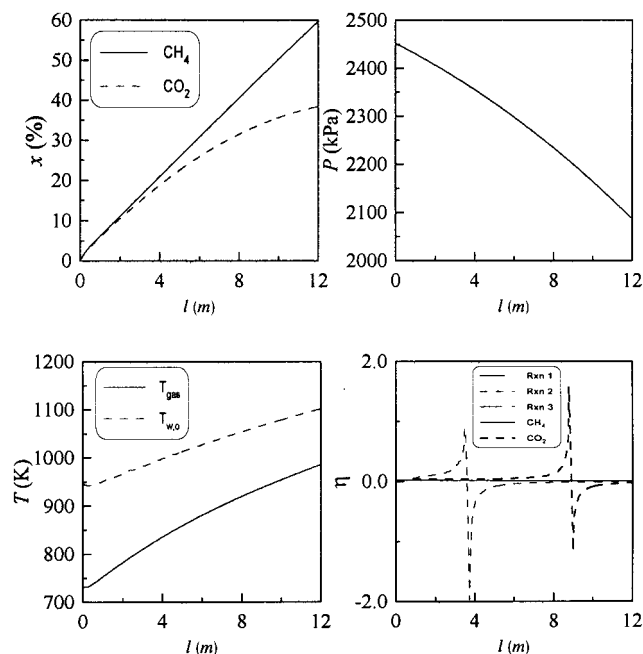


**Figure 2.** Simulation results for an industrial reformer. Values of variables and parameters as given in Table 3. Curves for  $\eta$  for reactions (1) and (3) are indistinguishable from that for  $\text{CH}_4$ .

plification of the flux equations. A summary of the model equations is given in Appendix 1, and a list of all parameters used in this study is given in Table 3. Additional details on the model are not being provided here because the model is only slightly different from that available in the open literature<sup>5,7,12</sup> and the changes made are obvious from the equations in Appendix 1.

The model equations are solved on a CRAY J916 supercomputer using the mathematical routines DIVPAG (for integration of the stiff ordinary differential equations<sup>22</sup>) and DNEQNF (for solving the nonlinear set of algebraic collocation equations) available in IMSL. Figure 2 shows the axial profiles of conversion, temperature, pressure, and effectiveness factors for the simulated case. A very good match is observed between the results obtained from our simulation and published industrial data (Figure 6.34 of ref 5 and Figures 2 and 3 of ref 9) under the same operating conditions (Table 3).

**Multiobjective Optimization.** The operation of the side-fired reformer simulated above is now optimized. This is in contrast to the design stage optimization of a new reformer. It is assumed that the rate of production of hydrogen,  $F_{\text{H}_2,\text{unit}}$ , from the unit is equal to a fixed (desired) rate,  $F_{\text{H}_2,\text{des}}$ . Under these conditions, the economics of steam reformer operation is governed by three main factors<sup>23</sup>—the cost of the feed, the cost of the additional furnace fuel, and the price that the export steam can fetch—all three of which are *unit-specific*. It is, therefore, necessary to perform a multiobjective function optimization with these three flow rates as simultaneous objectives. There is an inherent tradeoff between feed and fuel costs because maximizing the conversion of methane (which reduces the methane feed) lowers the heating value of the PSA off-gas, necessitating more external fuel. However, minimizing the input flow rate,  $F_{\text{CH}_4,\text{in}}$ , of methane also leads to a sizable reduction in the total fuel requirement. This is because lowering of the  $\text{CH}_4$  content in the feed decreases the rate of the endothermic reactions occurring in the reformer. In addition, industrial experience shows that

the feed costs usually dominate over fuel costs. This leaves only two *independent* objectives for study, namely, minimization of the flow rate of  $\text{CH}_4$  in the feed and maximization of the amount of steam exported. The second of these objectives can be further modified. A higher outlet temperature from the reformer results in a lower amount of unconverted methane in the off-gas (the reforming reactions being endothermic) and a higher amount of CO in the syngas (the reversible exothermic shift reaction being inhibited at high temperatures). The higher the CO in the syngas, the higher will be its exothermic conversion into  $\text{CO}_2$  in the shift converter. This would result in a higher temperature of the exit gases from the shift converter, leading, in turn, to an increase in the amount of steam that can be generated. In addition, Fischer–Tropsch and other downstream processes require syngas with as high a  $\text{CO}/\text{H}_2$  ratio as possible. Therefore, maximizing the flow rate,  $F_{\text{CO},\text{out}}$ , of CO in the syngas could be taken as the second objective (instead of the flow rate of the export steam). Thus, a meaningful optimization problem for the steam reforming of methane would be

$$\text{Min } I_1(\mathbf{u}) = F_{\text{CH}_4,\text{in}} \quad (4)$$

$$\text{Min } I_2(\mathbf{u}) = 10^8/F_{\text{CO},\text{out}} \quad (5)$$

where

$$\mathbf{u} = \{T_{\text{in}}, P_{\text{in}}, (\text{S/C})_{\text{in}}, (\text{H/C})_{\text{in}}, T_{\text{g}}, F\}$$

subject to (s.t.)

$$F_{\text{H}_2,\text{unit}} = F_{\text{H}_2,\text{des}} \quad (6)$$

$$T_{\text{w},0} \leq 1200 \text{ K} \quad (7)$$

It is to be emphasized here that the H in  $(\text{H/C})_{\text{in}}$  represents recycle hydrogen only and excludes the hydrogen present as steam [which is represented by  $(\text{S/C})_{\text{in}}$ ] and the hydrogen in the hydrocarbon feed. The empirical factor of  $10^8$  in eq 5 is used to give a similar range of values for  $I_1$  and  $I_2$  (and avoid numerical problems). In eqs 4 and 5,  $F_i$  represents the flow rate of component  $i$  at a specified location. The constraint on the outer wall temperature,  $T_{\text{w},0}$ , of the tube in eq 7 is based on the creep limit of alloy steel tubes at operating conditions and is required to avoid the rupture of tubes.

The following bounds are used for the decision variables

$$725 \leq T_{\text{in}} \leq 900 \text{ K} \quad (8)$$

$$2400 \leq P_{\text{in}} \leq 3000 \text{ kPa} \quad (9)$$

$$2.0 \leq (\text{S/C})_{\text{in}} \leq 6.0 \quad (10)$$

$$0.0 < (\text{H/C})_{\text{in}} \leq 0.5 \quad (11)$$

$$1375 \leq T_{\text{g}} \leq 1650 \text{ K} \quad (12)$$

$$2100 \leq F \leq 5000 \text{ kmol/h} \quad (13)$$

The lower limit on the gas temperature,  $T_{\text{in}}$ , at the reformer inlet is decided by thermodynamic limitations to prevent gum formation on the reformer catalyst. The upper limit on  $T_{\text{in}}$  is based on the maximum heat that the feed can normally pick up from the flue gases in the convection section of industrial reformers. The

minimum and the maximum values of the inlet pressure,  $P_{in}$ , have been decided based on respectively the normal pressures at which hydrogen is to be produced in the plant and the pressure of the natural gas. The lower limit of  $(S/C)_{in}$  is set at 2.0 to avoid carbon formation on the catalyst, which could occur at lower values. Very high  $(S/C)_{in}$  affects the process economics adversely because it involves the heating of the excess steam up to reforming (outlet) temperatures and subsequent condensation downstream of the reformer. The maximum  $(S/C)_{in}$  is usually limited to 6.0 in industrial practice. The maximum value of  $(H/C)_{in}$  is limited to 0.5 to avoid unnecessary recycle of  $H_2$  to the reformer. Bounds on the furnace gas temperature,  $T_g$ , have been fixed based on normal operating conditions of industrial reformer furnaces. The range of the total molar flow rate,  $F$ , has been limited to within 50 and 120% of the normal reformer flow rate because of turndown limitations and pressure drop considerations, respectively. It should be noted here that by fixing  $F$  we are not overspecifying the decision variables because  $(S/C)_{in}$  and  $(H/C)_{in}$  represent only molar ratios and not the molar flow rates of steam and recycle hydrogen.

The requirement of maintaining a desired rate of hydrogen production,  $F_{H_2,des}$ , from the PSA unit (taken as 3800 kg/h in this study) is incorporated as an endpoint constraint in eq 6. A common procedure for solving problems with such constraints is to use them in the form of penalty functions. The optimization problem studied finally is, thus,

$$\text{Min } I_1^*(\mathbf{u}) = F_{CH_4,in} + 10^6 \left( \frac{F_{H_2,des} - F_{H_2,unit}}{F_{H_2,des}} \right)^2 \quad (14)$$

$$\text{Min } I_2^*(\mathbf{u}) = \frac{10^8}{F_{CO,out}} + 10^6 \left( \frac{F_{H_2,des} - F_{H_2,unit}}{F_{H_2,des}} \right)^2 \quad (15)$$

s.t.

$$T_{w,0} \leq 1200 \text{ K} \quad (16)$$

with bounds on the decision variables as given in eqs 8–13.

In the present study, only the reformer has been modeled. Because  $F_{H_2,unit}$  is the hydrogen flow rate at the outlet of the PSA unit (after accounting for the  $H_2$  recycle), it is necessary to relate the flow rate of hydrogen at the exit of the reformer (as computed by the model equations) to  $F_{H_2,unit}$ . For this it has been assumed that 75% (molar basis) of the CO in the syngas (as predicted by the model) is converted into  $CO_2$  and  $H_2$  in the shift converter (as per eq 2 alone), consistent with typical values in industrial units.<sup>5</sup> In addition, it is assumed that the reformer furnace and steam generation equipment are designed to perform satisfactorily under the optimized (possibly more stringent) conditions.

The optimization problem described above is solved using an adapted version of genetic algorithm<sup>24</sup> suitable for multiobjective problems and referred to as the nondominated sorting genetic algorithm (NSGA).<sup>25,26</sup> This is described briefly in Appendix 2.

## Results and Discussion

The present optimization problem involves two objective functions which are influenced in opposite direc-

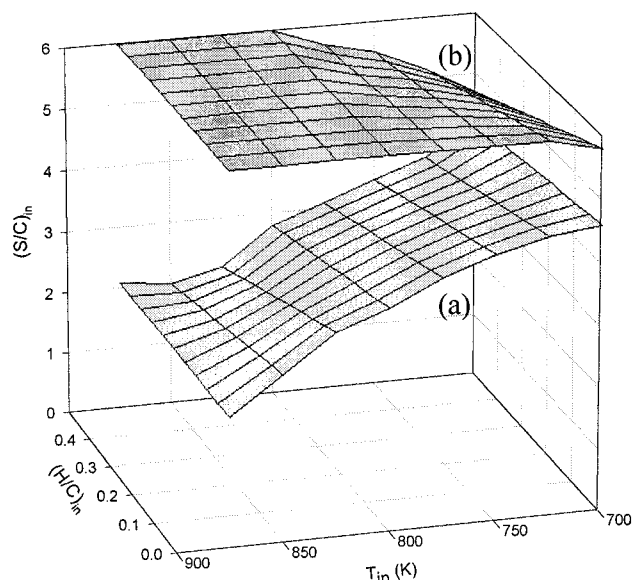
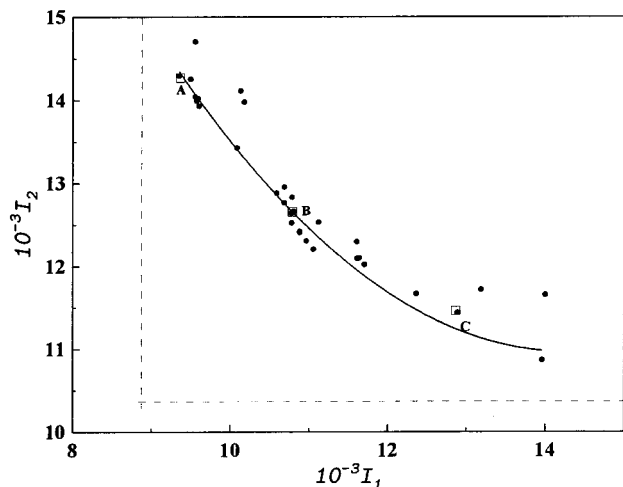


**Figure 3.** Domain of  $(S/C)_{in}$  for a choice of  $(H/C)_{in}$  and  $T_{in}$ . Parts a and b represent the lower and upper bounds on  $(S/C)_{in}$ .

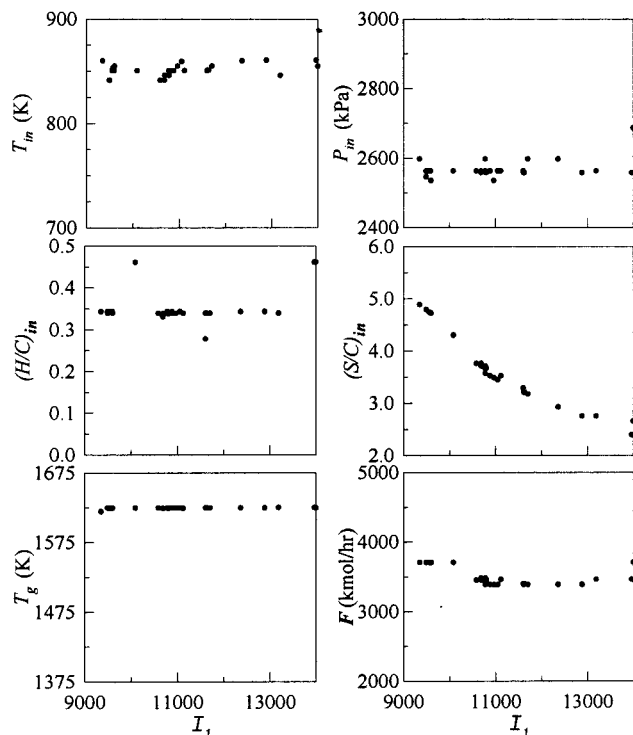
tions by changes in some of the decision variables. This leads to a situation wherein we obtain a set of nondominating solutions (Pareto-optimal solutions) rather than a unique solution. A Pareto set (for the present case of two objective functions) has the property that when we move from any one point to another on the set, one objective function improves but the other worsens. Hence, neither solution “dominates” over the other, and both are equally good (additional information is required to choose between them). Usually, a decision-maker selects a “preferred” point on the Pareto using his intuition, which is often nonquantifiable.

While the optimization was performed, it was found that for a given inlet temperature and  $(H/C)_{in}$ ,  $(S/C)_{in}$  had to be limited to within a certain region to prevent the intrapellet mole fractions from becoming negative during the iterative computations and to enable us to get solutions numerically. Figure 3 shows this domain. This has been generated using simulations under a whole variety of conditions. The mapping<sup>25,26</sup> of  $(S/C)_{in}$  from the binary chromosomes to the decimal system is to be done using *these* bounds rather than the ones in eq 10. It is obvious that the mapping of  $T_{in}$  and  $(H/C)_{in}$  needs to be done in the NSGA code before that for  $(S/C)_{in}$ . Such an adaptation was not required in previous multiobjective optimization studies using NSGA.<sup>25,26</sup>

Figure 4 shows the Pareto set of optimal solutions obtained. The CPU time taken to generate one Pareto set of optimal solutions is 41 min on the CRAY machine. The original objectives,  $I_1$  and  $I_2$ , are plotted rather than  $I_1^*$  and  $I_2^*$ . In fact,  $I_1^*$  and  $I_2^*$  are *almost* identical with  $I_1$  and  $I_2$ , respectively, on attainment of convergence. The dotted lines indicate the two asymptotes of the Pareto set and are obtained<sup>26</sup> by solving two single-objective optimization problems (using either  $I_1^*$  or  $I_2^*$ ). Each point (referred to as a chromosome) on the Pareto set is associated with a set of decision variables. These are shown in Figure 5. A small amount of scatter is observed both in the Pareto sets and in the decision variables. This could possibly be reduced by a slight modification of the computational parameters used in NSGA but was not considered necessary in view of the intensive nature of the computations involved.



**Figure 4.** Pareto-optimal set for a desired hydrogen production rate of 3800 kg/h. Points represent actual chromosomes, while the solid line represents a best-fit curve (after excluding far-flung points).



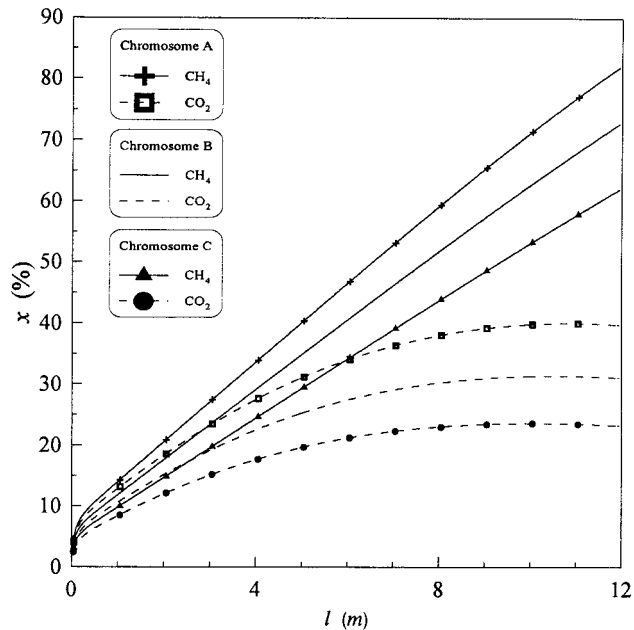
**Figure 5.** Decision variables corresponding to different points on the Pareto set of Figure 4.

Table 1 lists the decision variables corresponding to three chromosomes, A, B, and C, on the Pareto set of Figure 4. The conversion, temperature, and pressure profiles for operation of the reformer under these three Pareto-optimal conditions are shown in Figures 6–8, respectively. The variation of the effectiveness factors for the reactions and individual components along the axial location of the reformer tube for conditions corresponding to chromosome A is shown in Figure 9. From an analysis of the model, it can be inferred that excessive quantities of steam in the feed favor the forward reactions, leading to higher conversions of methane. However, more steam also results in reaction (3) dominating over reaction (1), lowering the CO in the reformer outlet. Similarly, large amounts of recycle hydrogen will inhibit reaction (3) and, to a lesser extent,

**Table 1.** Decision and Process Variables for a Few Chromosomes of the Pareto Sets in Figures 4 and 11

parameter	chr. A <sup>a</sup>	chr. B <sup>a</sup>	chr. C <sup>a</sup>	chr. P <sup>b</sup>	point Q <sup>b</sup>
Decision Variables					
$T_{in}$ (K)	841.7	851.1	861.0	859.5	733.0
$P_{in}$ (kPa)	2548.8	2559.8	2559.5	2740.3	2452.1
$(H/C)_{in}$	0.34	0.34	0.34	0.40	0.25
$(S/C)_{in}$	4.80	3.68	2.76	4.01	4.6
$T_g$ (K)	1625.0	1624.9	1625.0	1578.0	1575.0
$F$ (kmol/h)	3712.1	3463.1	3391.8	3751.2	4226.9
Process Variables					
$F_{CH_4,in}$ (kg/h)	9497.0	10803.5	12884.3	10871.8	11348.5
$F_{CO,out}$ (kg/h)	7014.9	7894.9	8742.5	6146.4	3898.2
$F_{H_2,out}$ (kg/h)	3767.2	3802.1	3841.8	3454.9	3449.5

<sup>a</sup> Figure 4. <sup>b</sup> Figure 11.



**Figure 6.** Conversion profiles of CH<sub>4</sub> and CO<sub>2</sub> for chromosomes A, B, and C of Figure 4.

reactions (1) and (2). This will reduce the conversion of methane and generate more CO in the product gas. Hence, a combination of high  $(S/C)_{in}$  and low  $(H/C)_{in}$  should require lower feed rates of methane, while low  $(S/C)_{in}$  and high  $(H/C)_{in}$  should give larger quantities of carbon monoxide at the reformer outlet. The reforming reactions are enhanced by operating the unit at lower pressures, while the shift reaction is unaffected by pressure variations. Therefore, the optimized solutions should predict operation close to the lower bound on the inlet pressure (2400 kPa). The Pareto-optimal set is consistent with these intuitive expectations, as is reflected from Figures 4 and 5. It was, however, observed that the effect of  $(S/C)_{in}$  dominated over that of  $(H/C)_{in}$  with increasing generation number.

The observed optimal values of the other five decision variables [except  $(S/C)_{in}$ ] are relatively invariant [compared to  $(S/C)_{in}$ ] among the various chromosomes (Figure 5). This may induce us to reconsider the need for framing a multivariable optimization problem. However, it should be noted that Figure 5 is for a particular case, i.e., for a specified maximum value for the tube wall temperature, a desired H<sub>2</sub> production rate and a prescribed value of the catalyst activity. Hence, whenever any of these operational constraints are altered, the optimal values of the other decision variables change, as is observed from Table 2 (described later). It should

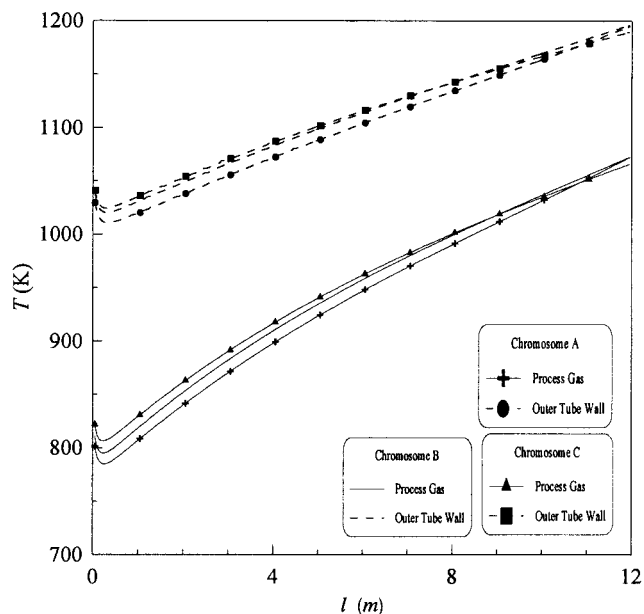


**Figure 7.** Process gas and tube wall temperature profiles for chromosomes A, B, and C of Figure 4.

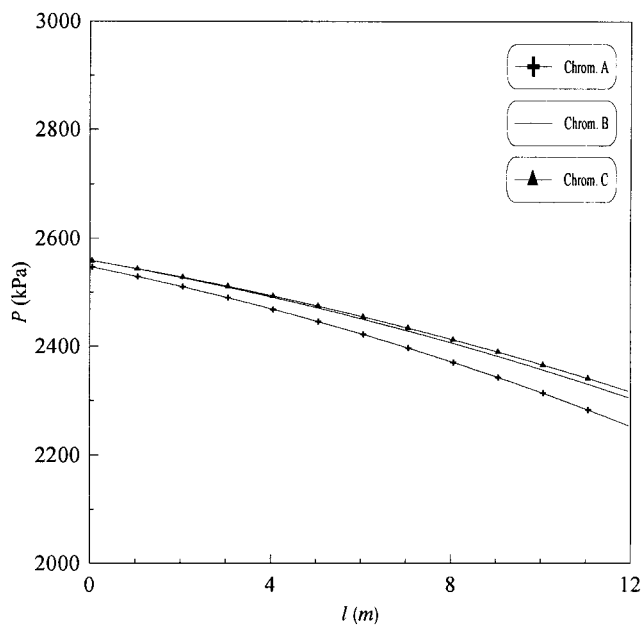


**Figure 8.** Pressure profiles for chromosomes A, B, and C of Figure 4.

also be stated that the three operating constraints mentioned above are subject to change over the short- and long-term operation of the unit. By performing a single-variable optimization, one would be unable to obtain optimal values of these other five decision variables for every new operating scenario. The present work, by carrying out optimization of all six decision variables, provides extra degrees of freedom for the optimization, resulting in more improved solutions than would have been possible if a single-variable search had been performed.

The maximum value of the outer tube wall temperature,  $T_{w,o}$ , limits the maximum possible exit temperature of the process gas. The exit temperature, in turn, influences the extent of the reforming and shift conversion reactions and thereby the objective functions. The exit temperature is itself controlled by the inlet temperature of the feed and the furnace temperature.

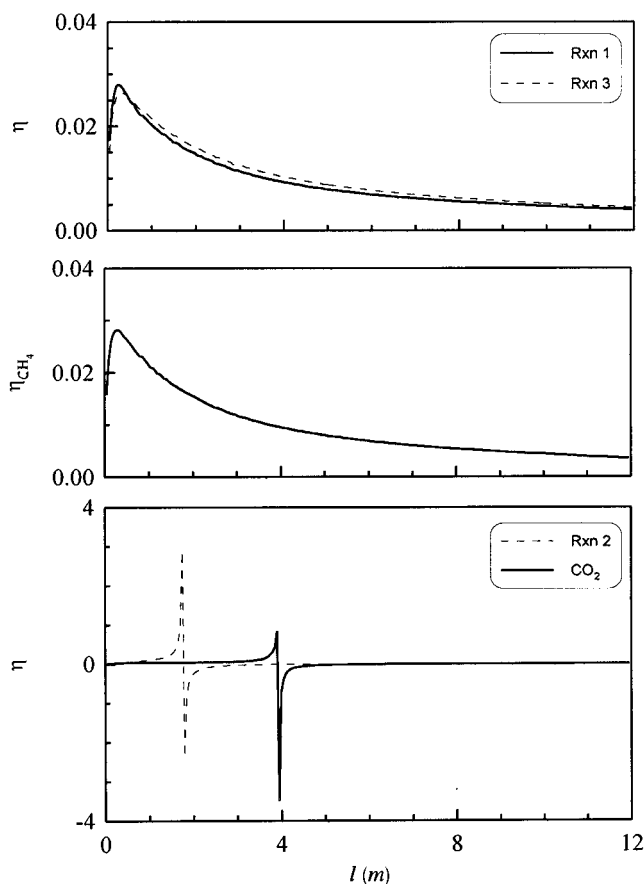


**Figure 9.** Profiles of the reaction and component effectiveness factors for chromosome A in the Pareto set of Figure 4.

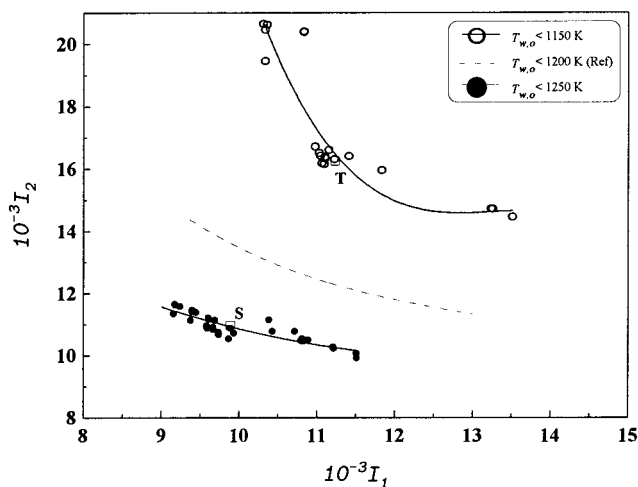
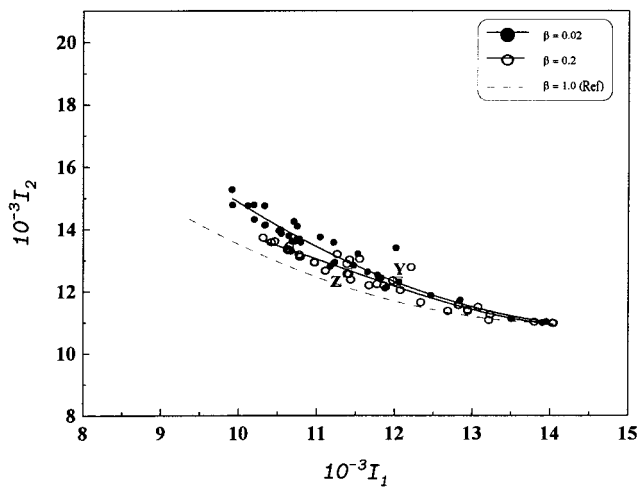
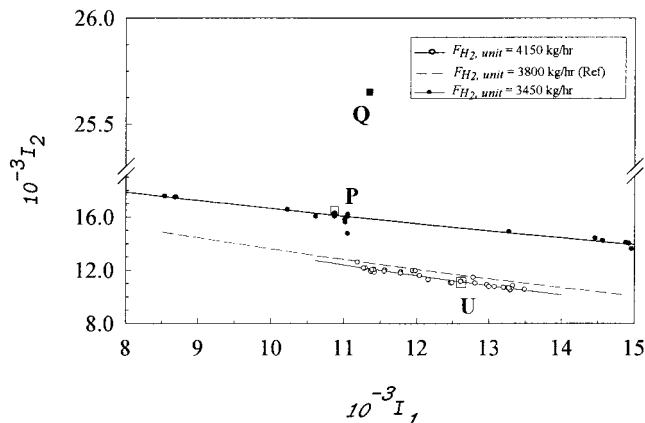
Reformers are usually operated near the highest allowable exit temperatures, where the reforming reactions are favored and the shift conversion reaction suppressed. It is also expected that the optimized solutions should have low feed rates, which will allow more heat to be picked up for a given furnace duty. The results of the present optimization study confirm these predictions by suggesting operation at high  $T_{in}$ ,  $T_g$ , and low  $F$  (refer to Figure 5). From Figure 7, it can be seen that the choice of  $T_{in}$  and  $T_g$  in most chromosomes is such that  $T_{w,o}$  is very close to the maximum possible limit. Similarly, Figure 8 shows a preference for operation at the lower range of pressures.

The sensitivity of the Pareto to the operational constraint on the maximum allowable tube (outer) wall temperature is shown in Figure 10. It follows from the earlier discussion that higher tube wall temperatures allow higher conversions of methane, resulting in lower  $F_{CH_4,in}$  and higher  $F_{CO,out}$ . This is borne out by the observed shift of the Pareto to higher  $I_1$  and  $I_2$  values. This shift is significant because reformers are operated in such a way that the maximum tube wall temperature decreases with the age of the tubes. Figure 10 can be used to change the operating point of a reformer with time, as the tube wall material ages.

Figure 11 shows the variation of the Pareto-optimal set with changes in  $F_{H_2,des}$ . We observe a shift of the Pareto-optimal set along the diagonal, with a change in  $F_{H_2,des}$ . This is in line with the reasoning that higher hydrogen production requires more  $F_{CH_4,in}$ , which can also give more  $F_{CO,out}$  in the product. An engineer can choose optimal operating conditions corresponding to the desired hydrogen production rate. One of the values

**Table 2. Decision and Process Variables for the Chromosomes of the Pareto Sets in Figures 10–13**

parameter	Chr. S	Chr. T	Chr. U	Chr. P	Chr. W	Chr. X	Chr. Y	Chr. Z
Decision Variables								
$T_{in}$ (K)	871.4	853.4	843.0	859.5	816.0	865.9	803.5	794.0
$P_{in}$ (kPa)	2520.1	2525.4	2460.5	2740.3	2631.9	2476.9	2525.8	2475.9
$(H/C)_{in}$	0.236	0.430	0.332	0.40	0.499	0.452	0.498	0.448
$(S/C)_{in}$	3.52	4.65	3.26	4.01	3.88	2.85	3.29	3.43
$T_g$ (K)	1644.5	1603.3	1655.6	1578.0	1641.5	1622.7	1641.6	1640.3
$F$ (kmol/h)	3008.52	4342.6	3703.7	3751.2	3819.2	3329.3	3633.0	3578.2
Process Variables								
$F_{CH_4,in}$ (kg/h)	9886.0	11224.1	12608.4	10871.8	11145.8	12074.0	12062.3	11472.3
$F_{CO,out}$ (kg/h)	9186.4	6128.5	8955.0	6146.4	7797.6	8846.4	8263.1	7786.2
$F_{H_2,unit}$ (kg/h)	3767.2	3801.5	4174.6	3454.9	3851.9	3774.0	3799.2	3727.6
Figure	10	10	11	11	13	13	12	12

**Figure 10.** Sensitivity of the Pareto to changes in the maximum value of the outer tube wall temperature.**Figure 12.** Effect of catalyst deactivation on the optimal solutions.  $k_I$ ,  $k_{II}$ , and  $k_{III}$  have been divided by factors of 5 and 50 for deactivated catalysts (equilibrium constants and diffusivity coefficients are unchanged).**Figure 11.** Variation of the Pareto with the desired hydrogen production rate. The Pareto for  $F_{H_2,des} = 3450$  kg/h allows an error of  $\pm 1\%$  because of the use of the penalty function.

selected for  $F_{H_2,des}$  (3450 kg/h) in Figure 11 is the same as that for the industrial reformer simulated by El-nashaie and co-workers<sup>5,9</sup> (and for which Figure 2 applies). It is interesting to analyze the operation of this reformer with respect to its optimality. The *actual*<sup>6</sup> feed rate of methane in the industrial reactor is 11 348 kg/h, while it produces 3898 kg/h of CO at the reformer outlet (shown as point Q in Figure 11). One of the possible sets of optimal operating conditions would, for the same  $H_2$  production rate, require only 10 872 kg/h of methane and will produce 6146 kg/h of CO (at the outlet of the reformer), corresponding to point P in Figure 11. Point P was selected because *both* of these values represent considerable improvements over the

values for the simulated industrial reactor. The values of the six decision variables corresponding to point P in Figure 11 are compared with those for the industrial reformer (point Q) in Table 1. It may be noted that the optimal point, P, is associated with a high value of  $T_{in}$  and a low  $F$ . These dominate over the effects of  $(H/C)_{in}$  and  $(S/C)_{in}$ . The higher value of  $P_{in}$  for point P over that of point Q is to satisfy the constraint on the outer wall temperature.

Industrial catalysts lose their activity with time because of undesirable processes such as poisoning, sintering, fouling, and aging. Therefore, it is important to study the effect of catalyst deactivation on optimal conditions for the operation of the unit. Figure 12 shows the shift of the Pareto for reduction in the activity of the catalyst which is assumed, in this work, to be caused only by poisoning or aging—by reducing  $k_I$ ,  $k_{II}$ , and  $k_{III}$  by a constant factor,  $\beta$ . The optimal conditions for the same processing objectives are observed not to change too much because of catalyst deactivation with the passage of time. This is not surprising because the process is controlled more by thermodynamics than by kinetics. However, a slight deterioration of objective function values with loss of activity can indeed be observed in line with the industrial measurements.<sup>2</sup>

The catalyst-filled reformer tubes often have their bed (external) void fraction,  $\epsilon_b$ , change during the course of normal operation because of several causes—thermal expansion/contraction of the tubes, breakage of the catalyst pellet, and gum formation on the catalyst surface. Even small changes in  $\epsilon_b$  can affect optimal

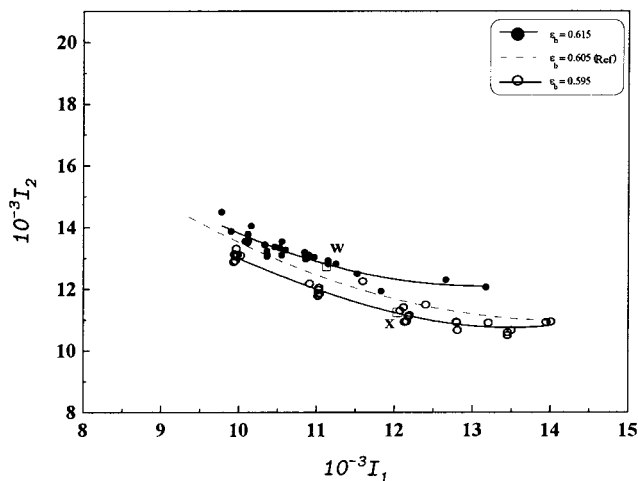


Figure 13. Effect of bed void fraction,  $\epsilon_b$ , on optimal solutions.

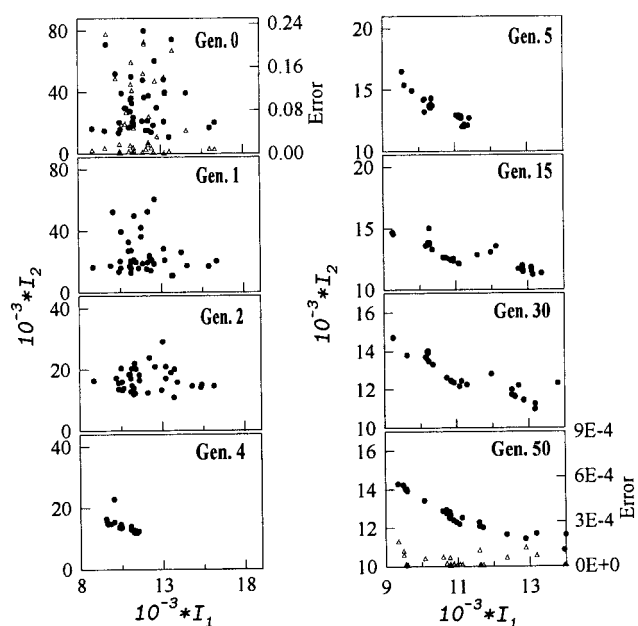


Figure 14. Evolution of the Pareto with generation number. The error is defined to be  $[1 - (F_{H_2, \text{unit}}/F_{H_2, \text{des}})]^2$ . Filled circles represent  $10^{-3}I_2$ , while triangles represent the associated error.

operation because of its very strong influence on the pressure drop and hence on the equilibrium conditions at the reformer outlet. To estimate this effect, optimization was performed at two values of  $\epsilon_b$  other than the reference case. As can be seen from Figure 13, higher values of  $\epsilon_b$  result in a worsening of both the objective functions while lower values of  $\epsilon_b$  improve both of the objective functions. This is expected because higher  $\epsilon_b$  give lower pressure drops, resulting in higher outlet pressures. The higher outlet pressure results in a shift of the equilibrium away from the products, resulting in a poorer performance of the reformer. The reverse is true for lower  $\epsilon_b$ .

During the course of our study it was found that the results were dependent to a good extent on the choice of some of the computational parameters. Figure 14 shows the change in the two objective functions over the generations for the reference case shown in Figure 4. The higher the generation number, the lesser is the scatter of the Pareto, and the lower is the deviation of  $F_{H_2, \text{unit}}$  from  $F_{H_2, \text{des}}$ . The effects of the crossover and mutation probabilities,  $p_c$  and  $p_m$ , respectively, on the

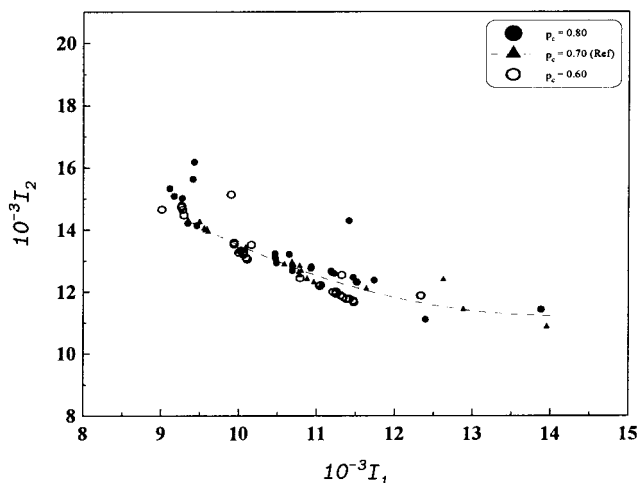


Figure 15. Influence of crossover probability on the Pareto.

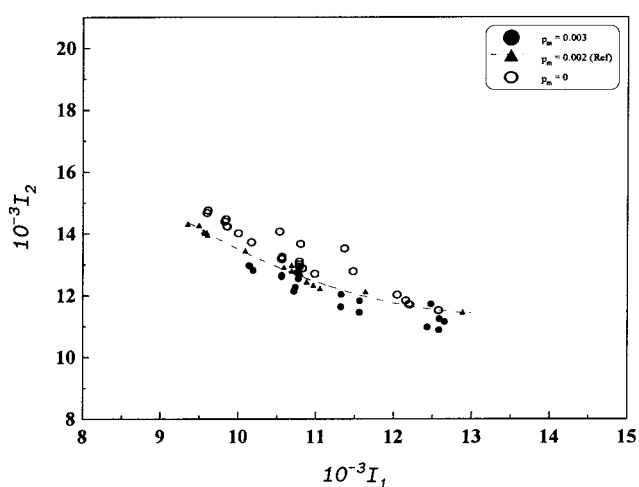


Figure 16. Influence of mutation probability on the Pareto.

Pareto set are shown in Figures 15 and 16. The actual points obtained show quite some scatter. It may be emphasized that the amount of scatter could be reduced to some extent by varying some of the other parameters in NSGA, but this was not done because the computations are quite time consuming, and we also wished to show that one must be careful in choosing the right set of computational parameters to obtain a smooth Pareto. Indeed, the parameters used to obtain the reference Pareto set (Figure 4) as well as those in Figures 10–13 were obtained after considerable effort to minimize their scatter. The same was *not* done in Figures 15 and 16 purely to give a glimpse of the worst-case scenario. Indeed, for values of  $p_m$  between 0.002 and 0.003, a *much* larger scatter was observed. One has to be quite careful to obtain a smooth Pareto.

Once the Pareto set is obtained, an engineer can choose to operate the reformer at the set of operating conditions corresponding to any one of the Pareto points using his/her operating experience, judgment, or other information that has not been incorporated while generating the optimal solutions (e.g., economic considerations). A single point on the Pareto (referred to as the preferred solution) is usually chosen for operation. This point is often arrived at by having several plant personnel rate the Pareto points according to their preferences and then taking a weighted average of their choices.<sup>27</sup> It should be noted that the present study describes the solution of a general optimization problem, suitable for

all plants, by excluding cost factors. The latter, though very important, are region-dependent (e.g., natural gas may be cheaper than HP steam in some areas, whereas the reverse may be true in other places). The use of cost optimization would limit the scope of our work, which is why optimization was based on process flow rates rather than on cash flows.

It may be added that, for reasons of brevity, the optimal values of the decision variables corresponding to several different points on the Paretos in Figures 10–13 are not provided herein. However, Table 2 provides the details for one selected point on each of the Paretos. Detailed results similar to those shown in Figure 5 for each of the Paretos can be supplied on request.

## Conclusions

The present study aims at demonstrating the possibility of enhancing the productivity of an existing industrial steam reformer by performing a multiobjective optimization. To this end, a mathematical model that is rigorous enough to satisfactorily characterize reformer operation over the range of possible operating conditions has been used. It is clear that there is a good potential for tapping more value from existing reformers by operating them at optimal conditions. Such operation will result in reduced operating costs, enhanced productivity, and increased profits.

## Nomenclature

$a$  = fraction of half catalyst pellet thickness in which the concentrations change  
 $A_f$  = surface area of the flame produced by a single burner ( $m^2$ )  
 $A_{t,i}$  = total internal surface area of all of the tubes ( $m^2$ )  
 $A_{t,o}$  = total external surface area of all of the tubes ( $m^2$ )  
 $A_{ref}$  = surface area of the refractory ( $m^2$ )  
 $C_p$  = specific heat of the process gas (kcal/kmol/K)  
 $d_i^i$  = internal diameter of the tube (m)  
 $d_o$  = external diameter of the tube (m)  
 $D_i^f$  = effective diffusivity of component  $i$  in the catalyst at any axial location ( $m^2/h$ )  
 $D_p$  = equivalent diameter of the catalyst pellet (Raschig ring) (m)  
 $(D/C)_{in}$  = carbon dioxide/methane molar ratio in the feed  
 $E$  = defined in eq A13  
 $F$  = reformer feed rate (kmol/h)  
 $F_{CH_4}$  = flow rate of methane at any axial location in the reformer tubes (kg/h)  
 $F_{CO_2}$  = flow rate of carbon dioxide at any axial location in the reformer tubes (kg/h)  
 $F_{H_2,des}$  = desired flow rate of hydrogen from the unit (kg/h)  
 $F_{H_2,unit}$  = actual flow rate of hydrogen from the unit (kg/h)  
 $G$  = mass velocity of the process gas (kg/h/ $m^2$ )  
 $(H/C)_{in}$  = recycle hydrogen/methane molar ratio in the feed  
 $l$  = axial location in the reformer tube (m)  
 $l_c$  = characteristic length of the catalyst pellet (m)  
 $L$  = total length of the reformer tube (m)  
 $k_I, k_{III}$  = rate constants of reactions (I) and (III) [kmol (kPa) $^{0.5}$ /kg of catalyst/h]  
 $k_{II}$  = rate constant of reaction (II) (kmol/kg of catalyst/h/kPa)  
 $K_g$  = thermal conductivity of the process gas at any axial location (kcal/h/m/K)  
 $K_I, K_{II}$  = equilibrium rate constants of reactions (I) and (II)  
 $K_i$  = equilibrium adsorption constants for component  $i$  (kPa $^{-1}$ ),  $i = CH_4, H_2, CO$   
 $K_{H_2O}$  = equilibrium adsorption constant for  $H_2O$   
 $K_w$  = thermal conductivity of the tube wall (kcal/h/m/K)

$M$  = number of internal collocation points  
 $N_b$  = number of burners in the reformer furnace  
 $(N/C)_{in}$  = nitrogen/methane molar ratio in the feed  
 $P$  = pressure at any axial location in the reformer tube (kPa)  
 $p_c$  = probability of crossover  
 $p_m$  = probability of mutation  
 $q_{cond}$  = conductive heat flux based on an average surface area of the tubes (kcal/h/ $m^2$ )  
 $q_{conv}$  = convective heat flux based on the inner surface area of the tubes (kcal/h/ $m^2$ )  
 $q_{rad}$  = radiative heat flux based on the outer surface area of the tubes (kcal/h/ $m^2$ )  
 $r_I, r_{II}, r_{III}$  = rate of reactions (I), (II), and (III) at the catalyst surface at any axial location (kmol/h/kg of catalyst)  
 $r_{CH_4}, r_{CO_2}, r_{H_2O}$  = rate of reaction of  $CH_4, CO_2,$  and  $H_2O$  at the catalyst surface at any axial location (kmol/h/kg of catalyst)  
 $r_{CH_4,n}, r_{H_2O,n}$  = rate of reaction of  $CH_4$  and  $H_2O$  at the  $n$ th collocation point in the catalyst pellet (kmol/h/kg of catalyst)  
 $R$  = sum of the molar ratios in the feed  
 $(S/C)_{in}$  = steam/methane molar ratio in the feed  
 $T$  = process gas temperature at any axial location in the reformer tube (K)  
 $T_f$  = adiabatic flame temperature (K)  
 $T_g$  = temperature of the furnace gas (K)  
 $T_{w,i}$  = temperature of the inner tube wall (K)  
 $T_{w,o}$  = temperature of the outer tube wall (K)  
 $U$  = overall heat-transfer coefficient [kcal/(h  $m^2$  K)]  
 $v$  = dimensionless distance within the half thickness of the catalyst pellet ( $v = 0$  at catalyst surface)  
 $x_{CH_4}$  = conversion of methane at any axial location =  $[(F_{CH_4,in} - F_{CH_4})/F_{CH_4,in}]$   
 $x_{CO_2}$  = conversion of carbon dioxide at any axial location =  $[(F_{CO_2} - F_{CO_2,in})/F_{CH_4,in}]$   
 $y_i$  = mole fraction of the component  $i$  in the bulk gas at any axial location  
 $\bar{y}_{i,n}$  = mole fraction of component  $i$  at the  $n$ th collocation point inside the catalyst pellet at any axial location

## Greek Symbols

$\beta$  = multiplication factor for the three forward rate constants to account for catalyst deactivation  
 $\rho_b$  = bulk density of the catalyst (kg/ $m^3$ )  
 $\rho_g$  = density of the gas mixture at any axial location (kg/ $m^3$ )  
 $\rho_s$  = catalyst density (kg/ $m^3$ )  
 $\mu$  = viscosity of the gas mixture at any axial location (kg/m/h)  
 $\eta_I, \eta_{II}, \eta_{III}$  = effectiveness factor for reactions (I), (II), and (III) at any axial location  
 $\eta_{CH_4}, \eta_{CO_2}$  = effectiveness factors for conversion of  $CH_4$  and  $CO_2$  at any axial location  
 $\epsilon_b$  = void fraction of the catalyst bed  
 $\epsilon_c$  = porosity of the pellet  
 $\tau$  = tortuosity of the pellet  
 $\xi_g$  = emissivity of the furnace gas  
 $\xi_f$  = emissivity of the flames  
 $\xi_t$  = emissivity of the tube material  
 $\sigma$  = Stefan–Boltzmann constant (kcal/h/ $m^2K^4$ )  
 $(-\Delta H_i)$  = heat of the  $i$ th reaction (kcal/kmol)  
 $\phi_s$  = sphericity of the catalyst pellet

## Subscripts

in = at the inlet of the reformer (after mixing with steam and recycle hydrogen)  
 out = at the outlet of the reformer (ahead of the shift converter)

unit = at the outlet of the entire plant (after the PSA unit)

### Appendix 1. Complete Set of Equations for the Steam Reforming Process

$$F_{\text{CH}_4, \text{in}} = 16 \frac{F}{R} \text{ where } R = [1 + (\text{S/C})_{\text{in}} + (\text{H/C})_{\text{in}} + (\text{D/C})_{\text{in}} + (\text{N/C})_{\text{in}}] \quad (\text{A1})$$

$$F_{\text{CO}_2, \text{out}} = 28 \frac{F(x_{\text{CH}_4, \text{out}} - x_{\text{CO}_2, \text{out}})}{R} \quad (\text{A2})$$

$$F_{\text{H}_2, \text{unit}} = 2 \frac{F(3.75x_{\text{CH}_4, \text{out}} + 0.25x_{\text{CO}_2, \text{out}})}{R} \quad (\text{A3})$$

#### (a) Kinetic Model.

$$\frac{dx_{\text{CH}_4}}{dl} = \left( \frac{\pi d_i^2}{4} \right) \frac{R \rho_b \eta_{\text{CH}_4} r_{\text{CH}_4}}{F}; \quad x_{\text{CH}_4} = 0 \text{ at } l = 0 \quad (\text{A4})$$

$$\frac{dx_{\text{CO}_2}}{dl} = \left( \frac{\pi d_i^2}{4} \right) \frac{R \rho_b \eta_{\text{CO}_2} r_{\text{CO}_2}}{F}; \quad x_{\text{CO}_2} = 0 \text{ at } l = 0 \quad (\text{A5})$$

$$\frac{dP}{dl} = - \frac{1.75 G^2 (1 - \epsilon_b)}{\phi_s D_p \epsilon_b^3 \rho_g}; \quad P = P_{\text{in}} \text{ at } l = 0 \quad (\text{A6})$$

$$r_{\text{CH}_4} = r_{\text{I}} + r_{\text{III}} \quad (\text{A7})$$

$$r_{\text{CO}_2} = r_{\text{II}} + r_{\text{III}} \quad (\text{A8})$$

$$r_{\text{H}_2\text{O}} = r_{\text{I}} + r_{\text{II}} + 2r_{\text{III}} \quad (\text{A9})$$

$$r_{\text{I}} = \frac{k_{\text{I}}}{E^2 y_{\text{H}_2}^{2.5} \sqrt{P}} \left( y_{\text{CH}_4} y_{\text{H}_2\text{O}} - \frac{P^2 y_{\text{H}_2}^3 y_{\text{CO}}}{K_{\text{I}}} \right) \quad (\text{A10})$$

$$r_{\text{II}} = \frac{k_{\text{II}} P}{E^2 y_{\text{H}_2}} \left( y_{\text{CO}} y_{\text{H}_2\text{O}} - \frac{y_{\text{H}_2} y_{\text{CO}_2}}{K_{\text{II}}} \right) \quad (\text{A11})$$

$$r_{\text{III}} = \frac{k_{\text{III}}}{E^2 y_{\text{H}_2}^{3.5} \sqrt{P}} \left( y_{\text{CH}_4} y_{\text{H}_2\text{O}}^2 - \frac{y_{\text{H}_2}^4 y_{\text{CO}_2}}{K_{\text{I}} K_{\text{II}}} \right) \quad (\text{A12})$$

$$E = \left[ 1 + P(K_{\text{CO}} y_{\text{CO}} + K_{\text{CH}_4} y_{\text{CH}_4} + K_{\text{H}_2} y_{\text{H}_2}) + K_{\text{H}_2\text{O}} \frac{y_{\text{H}_2\text{O}}}{y_{\text{H}_2}} \right] \quad (\text{A13})$$

$$y_{\text{CH}_4} = \frac{(1 - x_{\text{CH}_4})}{[R + 2x_{\text{CH}_4}]} \quad (\text{A14})$$

$$y_{\text{H}_2\text{O}} = \frac{((\text{S/C})_{\text{in}} - x_{\text{CH}_4} - x_{\text{CO}_2})}{[R + 2x_{\text{CH}_4}]} \quad (\text{A15})$$

$$y_{\text{CO}} = \frac{(x_{\text{CH}_4} - x_{\text{CO}_2})}{[R + 2x_{\text{CH}_4}]} \quad (\text{A16})$$

$$y_{\text{CO}_2} = \frac{((\text{D/C})_{\text{in}} + x_{\text{CO}_2})}{[R + 2x_{\text{CH}_4}]} \quad (\text{A17})$$

$$y_{\text{H}_2} = \frac{((\text{H/C})_{\text{in}} + 3x_{\text{CH}_4} + x_{\text{CO}_2})}{[R + 2x_{\text{CH}_4}]} \quad (\text{A18})$$

$$y_{\text{N}_2} = \frac{(\text{N/C})_{\text{in}}}{[R + 2x_{\text{CH}_4}]} \quad (\text{A19})$$

#### (b) Energy Balance.

$$\frac{dT}{dl} = \frac{1}{GC_p} \left\{ \frac{4U(T_{w,i} - T)}{d_i} + \rho_b \sum_{i=1}^{\text{III}} (-\Delta H_i) \eta_i r_i \right\}; \quad T = T_{\text{in}} \text{ at } l = 0 \quad (\text{A20})$$

Inner tube wall temperature  $T_{w,i}$  is obtained by equating the heat fluxes due to (i) radiative transfer from the furnace gases to the exterior surface of the tubes

$$q_{\text{rad}} = \sigma \frac{(A_{t,o} + A_{\text{ref}}) \xi_g \xi_t}{(A_{t,o} + A_{\text{ref}}) \xi_g + A_{t,o} (1 - \xi_g) \xi_t} (T_g^4 - T_{w,o}^4) + \frac{N_b A_{\text{ref}} \xi_t (1 - \xi_g)}{\sigma A_{t,o}} T_f^4 \quad (\text{A21})$$

(ii) conductive transfer through the tube material

$$q_{\text{cond}} = \frac{2K_w(T_{w,o} - T_{w,i})}{\ln(d_o/d_i)} \quad (\text{A22})$$

and (iii) convective transfer to the gas mixture and catalyst bed from the inner surface of the tubes

$$q_{\text{conv}} = U(T_{w,i} - T) \quad (\text{A23})$$

$$U = 0.4 \frac{K_g}{D_p} \left\{ 2.58 \left( \frac{D_p G}{\mu} \right)^{1/3} \left( \frac{C_p \mu}{K_g} \right)^{1/3} + 0.094 \left( \frac{D_p G}{\mu} \right)^{0.8} \left( \frac{C_p \mu}{K_g} \right)^{0.4} \right\} \quad (\text{A24})$$

#### (c) Diffusion Model.

$$\eta_k = \frac{\int_{v=0}^{v=a} r_k(\bar{y}_p, T, P) dv}{r_k(\bar{y}_p, T, P) l_c} \quad k = \text{I, II, and III} \quad (\text{A25})$$

where  $\bar{y}_{i,n}$  are obtained by solving the coupled set of  $5(M - 1)$  equations:  $3(M - 1)$  algebraic and  $2(M - 1)$  differential (which are transformed into algebraic equations by orthogonal collocation on finite elements):

$$\frac{d^2 \bar{y}_{\text{CH}_4, n}}{dv^2} = a^2 l_c^2 \left\{ \frac{\rho_s (r_{\text{I}} + r_{\text{II}} + 2r_{\text{III}})_b}{(P/RT) D_{\text{CH}_4}^e} \right\} r_{\text{CH}_4, n} \quad n = 2, \dots, M + 1 \quad (\text{A26})$$

$$\frac{d^2 \bar{y}_{\text{H}_2\text{O}, n}}{dv^2} = a^2 l_c^2 \left\{ \frac{\rho_s (r_{\text{I}} + r_{\text{II}} + 2r_{\text{III}})_b}{(P/RT) D_{\text{H}_2\text{O}}^e} \right\} r_{\text{H}_2\text{O}, n} \quad n = 2, \dots, M + 1 \quad (\text{A27})$$

$$\bar{y}_{\text{CO}, n} = y_{\text{CO}} - \frac{1}{D_{\text{CO}}^e} [2D_{\text{CH}_4}^e (\bar{y}_{\text{CH}_4, n} - y_{\text{CH}_4}) - D_{\text{H}_2\text{O}}^e (\bar{y}_{\text{H}_2\text{O}, n} - y_{\text{H}_2\text{O}})] \quad n = 2, \dots, M + 1 \quad (\text{A28})$$

$$\bar{y}_{\text{CO}_2, n} = y_{\text{CO}_2} + \frac{1}{D_{\text{CO}_2}^e} [D_{\text{CH}_4}^e (\bar{y}_{\text{CH}_4, n} - y_{\text{CH}_4}) - D_{\text{H}_2\text{O}}^e (\bar{y}_{\text{H}_2\text{O}, n} - y_{\text{H}_2\text{O}})] \quad n = 2, \dots, M + 1 \quad (\text{A29})$$

**Table 3. Parameters Used in the Simulation of the Methane Steam Reformer**

parameter	value/specification	ref
Reformer Data		
heated length of reformer tubes, $L$	11.95 m	5
inside diameter of reformer tubes, $d_i$	0.0795 m	5
outside diameter of reformer tubes, $d_o$	0.102 m	5
ratio of reformer tube pitch to diameter	2.4	5
number of tubes	176	5
refractory surface area, $A_{ref}$	1164 m <sup>2</sup>	5
number of burners, $N_b$	112	5
flame surface area, $A_f$	0.01 m <sup>2</sup>	<i>a</i>
Catalyst Data		
catalyst shape	Raschig ring	5
catalyst pellet dimensions	16 × 6 × 16 mm	5
pellet porosity, $\epsilon_c$	0.51963	5
pellet sphericity, $\phi_s$	0.6563	5
pellet equivalent diameter, $D_p$	17.4131 mm	5
pellet tortuosity, $\tau$	2.74	5
solid catalyst density, $\rho_s$	2355.2 kg/m <sup>3</sup>	7
mean pore radius	80.0 Å	5
pellet characteristic length, $l_c$	1.948 mm	5
catalyst bed density, $\rho_b$	1362.0 kg/m <sup>3</sup>	5
catalyst bed void fraction, $\epsilon_b$	0.605	28
Other Data		
carbon dioxide to methane ratio, (D/C) <sub>in</sub>	0.091	5
nitrogen to methane ratio, (N/C) <sub>in</sub>	0.020	5
emmissivity of flames, $\xi_f$	0.1	29
emmissivity of furnace gases, $\xi_g$	0.1	29
emmissivity of reformer tubes, $\xi_t$	0.95	13
adiabatic flame temperature, $T_f$	2200 K	29
furnace gas temperature, $T_g$	1575 K	<i>a</i>
tube thermal conductivity, $K_w$ in W/(m K)	10.738 + 0.0242 $T_w$	13
no. of collocation points, $M + 2$	18	<i>b</i>
active fraction, $a$	0.2	<i>b</i>

<sup>a</sup> This work (typical industrial values used). <sup>b</sup> This work (obtained by trial to match reported results).

$$\bar{y}_{H_2,n} = y_{H_2} - \frac{1}{D_{H_2}^e} [2D_{CH_4}^e (\bar{y}_{CH_4,n} - y_{CH_4}) + D_{H_2O}^e (\bar{y}_{H_2O,n} - y_{H_2O})] \quad n = 2, \dots, M + 1 \quad (A30)$$

Boundary conditions:

$$\bar{y}_{i,1} = y_i \quad i = CH_4, H_2O, CO, CO_2, H_2 \quad (A31)$$

$$\frac{d\bar{y}_{i,M+2}}{dv} = 0 \quad i = CH_4, H_2O, CO, CO_2, H_2 \quad (A32)$$

Effectiveness factor for components are evaluated from reaction effectiveness factors

$$\eta_{CH_4} = \frac{\eta_I r_I + \eta_{III} r_{III}}{r_I + r_{III}} \quad (A33)$$

$$\eta_{CO_2} = \frac{\eta_{II} r_{II} + \eta_{III} r_{III}}{r_{II} + r_{III}} \quad (A34)$$

Correlations for  $C_p$ ,  $\mu$ , and  $K_g$  were obtained from HYSYS, while those given in ref 5 for  $\Delta H_i$ ,  $k_i$ ,  $K_i$ , and  $D_i^e$  were used. The gas mixture was assumed to be ideal in computing  $\rho_g$ . The average molecular weight and molar flow rate at the reformer inlet were used to compute  $G$ . Table 3 lists all parametric values used in this work.

## Appendix 2. Introduction to NSGA<sup>25,26</sup>

To solve multiobjective optimization problems, Srinivas and Deb<sup>25</sup> have developed an adaptation of the GA, namely, the NSGA. This algorithm generates a set of

**Table 4. NSGA Parameters and Their Values**

parameter	value
population size	50
no. of generations	50
length of chromosome	32 bits
crossover probability, $p_c$	0.70
mutation probability, $p_m$	0.002
spreading parameter, $\alpha$	2.0
spreading parameter, $\sigma$	0.05

solutions which are nondominating over each other. Two solutions are said to be nondominating if moving from one point to another results in an improvement in one of the objective functions but a deterioration in one (or more) of the other objective function(s). The final set of nondominating solutions is referred to as a Pareto optimal set. This algorithm differs from the traditional GA in the way the selection operator works. In the NSGA, prospective solutions are sorted into fronts—an imaginary enclosure within which all chromosomes are mutually nondominating—and such fronts are ranked progressively until all of the chromosomes are accounted for. Each chromosome is then assigned a fitness value obtained by sharing a dummy fitness value of the front by its niche count—a parameter proportional to the number of chromosomes in its neighborhood (in the decision variable space) within the same front. This helps spread out the chromosomes while maintaining the diversity of the gene pool. All other operations performed are similar to those in traditional GA's.<sup>24</sup> More details are available in refs 25 and 26. The relevant GA parameters used in this study are presented in Table 4.

## Literature Cited

- (1) Adris, A. M.; Pruden, B. B.; Lim, C. J.; Grace, J. R. On the Reported Attempts to Radically Improve the Performance of the Steam Reforming Reactor. *Can. J. Chem. Eng.* **1996**, *74*, 177.
- (2) Rostrup-Nielsen, J. R. Catalytic Steam Reforming. In *Catalysis—Science and Technology*; Anderson, A. R., Boudart, M., Eds.; Springer: Berlin, 1984; Vol. 5.
- (3) Ridler, D. E.; Twigg, M. V. Steam Reforming. In *Catalyst Handbook*; Twigg, M. V., Ed.; Wolfe: London, 1989.
- (4) Elnashaie, S. S. E. H.; Al-Ubaid, A. S.; Soliman, M. A.; Adris, A. M. On the Kinetics and Reactor Modelling of the Steam Reforming of Methane—A Review. *J. Eng. Sci.* **1988**, *14*, 247.
- (5) Elnashaie, S. S. E. H.; Elshishini, S. S. *Modelling, Simulation and Optimization of Industrial Catalytic Fixed Bed Reactors*; Gordon and Breach: Amsterdam, The Netherlands, 1993.
- (6) Xu, J.; Froment, G. F. Methane Steam Reforming, Methanation and Water—Gas Shift: I. Intrinsic Kinetics. *AIChE J.* **1989**, *35*, 88.
- (7) Xu, J.; Froment, G. F. Methane Steam Reforming: II. Diffusional Limitations and Reactor Simulation. *AIChE J.* **1989**, *35*, 97.
- (8) De Deken, J. C.; Devos, E. F.; Froment, G. F. Steam Reforming of Natural Gas: Intrinsic Kinetics, Diffusional Resistances and Reactor Design. *Chemical Reaction Engineering. ACS Symp. Ser.* **1982**, *196*, 181.
- (9) Elnashaie, S. S. E. H.; Adris, A. M.; Soliman, M. A.; Al-Ubaid, A. S. Digital Simulation of Industrial Steam Reformers for Natural Gas using Heterogeneous Models. *Can. J. Chem. Eng.* **1992**, *70*, 786.
- (10) Soliman, M. A.; Elnashaie, S. S. E. H., Al-Ubaid, A. S.; Adris, A. M. Simulation of Steam Reformers for Methane. *Chem. Eng. Sci.* **1988**, *43*, 1801.
- (11) Hyman, M. H. Simulate Methane Reformer Reactions. *Hydrocarbon Process.* **1968**, *47*, 131.
- (12) Singh, C. P. P.; Saraf, D. N. Simulation of Side Fired Steam-Hydrocarbon Reformers. *Ind. Eng. Chem., Process Des. Dev.* **1979**, *18*, 1.
- (13) Plehiers, P. M.; Froment, G. F. Coupled Simulation of Heat Transfer and Reaction in a Steam Reforming Furnace. *Chem. Eng. Technol.* **1989**, *12*, 20.
- (14) Trimm, D. L. Coke formation and minimization during steam reforming reactions. *Catal. Today* **1997**, *37*, 233.
- (15) Hossain, M. A. Best Conditions to Make Syngas. *Hydrocarbon Process.* **1988**, *67*, 76.
- (16) Elnashaie, S. S. E. H.; Adris, A. M.; Al-Ubaid, A. S.; Soliman, M. A. On the Nonmonotonic Behavior of Methane Steam Reforming Kinetics. *Chem. Eng. Sci.* **1990**, *45*, 491; **1994**, *49*, 1079.
- (17) Wagner, E. S.; Froment, G. F. Steam Reforming Analyzed. *Hydrocarbon Process.* **1992**, *71*, 69.
- (18) Zhang, S. W.; Yu, Y. G. Simulation, Analysis and Optimization of a Steam Reforming Process for a Large Scale Ammonia Plant. *Chin. J. Chem. Eng.* **1995**, *3*, 223.
- (19) Hohmann, F. W. Improve Steam Reformer Performance. *Hydrocarbon Process.* **1996**, *75*, 71.
- (20) Farnell, P. W. Modern Techniques for Optimization of Primary Reformer Operation. *Ammonia Plant Saf. Relat. Facil.* **1997**, *37*, 261.
- (21) Carey, G. F.; Finlayson, B. A. Orthogonal Collocation on Finite Elements. *Chem. Eng. Sci.* **1975**, *30*, 587.
- (22) Gupta, S. K. *Numerical Methods for Engineers*; Wiley Eastern/New Age Intl.: New Delhi, India, 1995.
- (23) *Topsøe Topics—Hydrogen*; Haldor Topsøe A/S: Lyngby, Denmark, Feb 1993.
- (24) Goldberg, D. E. *Genetic Algorithms in Search, Optimization and Machine Learning*; Addison-Wesley: Reading, MA, 1989.
- (25) Srinivas, N.; Deb, K. Multiobjective Optimization Using Nondominated Sorting in Genetic Algorithms. *Evol. Comput.* **1995**, *2*, 106.
- (26) Mitra, K.; Deb, K.; Gupta, S. K. Multiobjective Dynamic Optimization of an Industrial Nylon 6 Semibatch Reactor Using Genetic Algorithm. *J. Appl. Polym. Sci.* **1998**, *69*, 69.
- (27) Chankong, V.; Haimes, Y. Y. *Multiobjective Decision Making—Theory and Methodology*; Elsevier: New York, 1983.
- (28) Seader, J. D.; Henley, E. J. *Separation Process Principles*; Wiley: New York, 1997.
- (29) Hottel, H. C.; Sarrofm, A. F. *Radiative Heat Transfer*; McGraw-Hill: New York, 1967.

Received for review July 21, 1999

Revised manuscript received November 5, 1999

Accepted November 9, 1999

IE9905409